Structural Engineering and Mechanics, *Vol. 67, No. 4 (2018) 403-415*
DOI: https://doi.org/10.12989/sem.2018.67.4.403

Thermal effects on nonlinear dynamic characteristics of polymer-CNT-fiber multiscale nanocomposite structures

Farzad Ebrahimi* and Sajjad Habibi

Department of Mechanical Engineering, Faculty of Engineering, Imam Khomeini International University, Qazvin, Iran

(Received November 23, 2017, Revised May 21, 2018, Accepted June 12, 2018)

Abstract. In the present study, nonlinear dynamic response of polymer-CNT-fiber multiscale nanocomposite plate resting on elastic foundations in thermal environments using the finite element method is performed. In this regard, the governing equations are derived based on Inverse Hyperbolic Shear Deformation Theory and von Kármán geometrical nonlinearity. Three type of distribution of temperature through the thickness of the plate namely, uniform linear and nonlinear are considered. The considered element is C1-continuous with 15 DOF at each node. The effective material properties of the multiscale composite are calculated using Halpin-Tsai equations and fiber micromechanics in hierarchy. The carbon nanotubes are assumed to be uniformly distributed and randomly oriented through the epoxy resin matrix. Five types of impulsive loads are considered, namely the step, sudden, triangular, half-sine and exponential pulses. After examining the validity of the present work, the effects of the weight percentage of SWCNTs and MWCNTs, nanotube aspect ratio, volume fraction of fibers, plate aspect, temperature, elastic foundation parameters, distribution of temperature and shape of impulsive load on nonlinear dynamic response of CNT reinforced multi-phase laminated composite plate are studied in details.

Keywords: nonlinear dynamic response; multiscale nanocomposite; carbon nanotube; thermal environment; finite element method

1. Introduction

Due to unique properties carbon fiber reinforced polymers (CFRP) composites have been extensively employed in various structural applications and are suitable substitutes for traditional metals. Some characteristics such as fatigue and wear resistance, formability of complex shapes and high strength to weight ratio, increase a widespread use of CFRPs in industries which weight plays a great role, such as military, aerospace engineering, and automotive. Significant efforts in the research community have been carried out on enhancing CFRPs properties. On the other hand, combination of nanoparticles and macroscale matrices can present a novel type of composites with enhanced properties. Prior to discuss about the nanocomposite structures, the researchers are hugely advised to study about the nanomaterials (Alizada *et al*. 2012). Meanwhile, as powerful tools, numerical methods have been often used to solve related complicated equations (Civalek and Demir 2016). Carbon nanotubes (CNT) are an ideal candidate as nanoscale reinforcement for improvement of the multi functionality of CFRP composites. Their tensile strength of over 150 GPa and elastic modulus of over 1000 GPa make them very stronger and stiffer than steel while being three to five times lighter (Kim *et al*. 2009). Research groups have demonstrated that mechanical properties of composites can strongly increase by adding a few weight percent (wt.%) of CNTs (Spitalsky *et al.* 2010, Sahoo *et al.* 2010). Extraordinary properties such as high strength, high stiffness, high aspect ratio and low density of the CNT, makes it an opportunity for combining potential advantages of nanoscale reinforcement and functionality with well-accepted CFRPs to develop multiphase composites. Thermal and moisture analysis in structures and nanostructures has been one of the prominant subjects for many researchers (Ebrahimi and Barati 2016a-n, Ebrahimi and Barati 2017).

A research on the development of modern structural based on engineered CNTs/fiber/polymer multiphase composite is presented by Bekyarova *et al*. (2007). Godora *et al*. (2009) presented the effect of CNT reinforcement on the processing and the mechanical behavior of CFRP composites. They discussed the CNT dispersion and its stability during the processing steps and the characteristics of CFRPs. Thostenson *et al.* (2002) studied the effect of local nanotube reinforcement on load transfer at the fiber/matrix inter face of CNT multiphase composites. Green *et al.* (2009) studied synthesis, and thermo mechanical behavior of carbon nano fiber/epoxy nano phased polymer matrix.

Rafiee *et al.* (2014b) investigated nonlinear vibration of CNT multiphase laminated composites integrated with piezoelectric. In another work (Rafiee *et al*. 2014a) they using an analytical approach presented modeling and stress analysis of smart polymer/CNT/fiber composite plates. Nonlinear dynamic response and flexural of polymer/CNT/fiber multiphase nanocomposite plates are analyzed by Bhardwaj *et al*. (2013). They used double

*Corresponding author, Associate Professor
E-mail: febrahimy@eng.ikiu.ac.ir

ISSN: 1225-4568 (Print), 1598-6217 (Online)

Chebyshev polynomials to solve the problem. He *et al*. (2015) investigated large amplitude vibration of fractionally damped viscoelastic polymer/CNT/fiber nanocomposite beams.

Furthermore, a limited number of research works studied the dynamic response of the CNT reinforced composite. However, all of these studies are performed for two-phase CNT-reinforced polymeric composites. Yas and Heshmati (2012) presented dynamic analysis of functionally graded carbon nanotube reinforced composites beam under the action of moving load using the finite element method. Eshelby–Mori–Tanaka approach based on an equivalent fiber employed to estimate material properties of the beam. Also, they in another study (Heshmati and Yas 2013), investigated the dynamic behaviors of MWCNT-poly styrene beams subjected to multi-moving loads. Moradi-Dastjerdi *et al.* (2013) investigated dynamic analysis of carbon nanotube- reinforced functionally graded cylindrical panels subjected to an impact load using the mesh-free method. Wang and Shen (2012) analyzed the nonlinear dynamic response of temperature-dependent nanotube-reinforced composite plates on an elastic foundation under thermal by applying the rule of mixture. They used a two-step perturbation technique to solve the problem. Lei *et al.* (2015) carried out elasto-dynamic analysis of carbon nanotube-reinforced functionally graded plates. The governing differential equations were obtained using the first-order shear deformation plate theory, which were solved using the element-free kp-Ritz method.

There are many shear deformation plate theories have been proposed by researchers. Classical Laminated Plate Theory (CLPT) was developed based on the assumptions of Kirchhoff's plate theory which neglects the interlaminar shear deformation, and is less accurate. The first order shear deformation theory (FSDT) by Reissner (1945) and Mindlin (1951) proposed, assuming constant transverse shear deformation through the thickness of the plate. This theory does not satisfy the stress-free boundary conditions on the surfaces of the plate and requires a shear correction factor. To overcome these disadvantage, Reddy (1984) proposed a simple higher order theory for laminated plates which is free from any shear correction factor.

In the past the various polynomial and non-polynomial higher-order shear-deformation theories have been developed. The polynomial shear-deformation theories (PSDTs) were presented based on Taylor's series expansion of higher-order terms, and important works on PSDTs can be found in Levinson (1980), Lo *et al*. (1977), Reddy (2004), Kant and Pandya (1988), Talha and Singh (2010). In non-polynomial shear deformation theories, the in-plane displacements are the function of thickness coordinate, and developed by Murthy (1981), Soldatos (1992), Aydogdu (2009), Mantari *et al.* (2011) , (2012), and EL Meiche *et al.* (2011). Most recently, Grover *et al.* (2013) proposed new non-polynomial shear deformation theory with Inverse Hyperbolic function and applied for responses of laminated composite and sandwich plates.

To the best of author's knowledge, there is no analysis on the dynamic response of CNTs/fiber/polymer multi-phase composites in thermal environment have been carried out till now. Therefore, in the present study, Nonlinear dynamic response of polymer-CNT-fiber multiscale nanocomposite plate resting on elastic foundations in thermal environments using the finite element method is performed. In this regard, the governing equations are derived based on Inverse Hyperbolic Shear Deformation Theory (Grover *et al.* 2013) and von Kármán geometrical nonlinearity. Three type of distribution of temperature through the thickness of the plate namely, uniform linear and nonlinear are considered. The considered element is C^1-continuous with 15 DOF at each node. The effective material properties of the multiscale composite are calculated using Halpin-Tsai equations and fiber micromechanics in hierarchy. The carbon nanotubes are assumed to be uniformly distributed and randomly oriented through the epoxy resin matrix. Five types of impulsive loads are considered, namely the step, sudden, triangular, half-sine and exponential pulses.

After examining the validity of the present work, the effects of the weight percentage of SWCNTs and MWCNTs, nanotube aspect ratio, volume fraction of fibers, plate aspect, temperature, elastic foundation parameters, distribution of temperature and shape of impulsive on nonlinear dynamic response of CNT reinforced multi-phase laminated composite plate are studied in details.

2. Theoretical formulation

Fig. 1 shows a rectangular multiphase nanocomposite plate composed of isotropic matrix (epoxy resin), CNTs and fibers (carbon) on elastic foundation. Coordinate system and the geometric parameters used for the plate are depicted in Fig. 1.

2.1 Carbon nanotube/fiber/polymer multi-phase composite material model

The effective mechanical properties of these composites can be obtained based on a combination of Halpin-Tsai (Thostenson *et al*. 2002) and micromechanics approach scheme (Shen 2009), with two steps in the hierarchy as depicted in Fig. 2. The resulting properties of the CNT reinforced multi-phase laminated composite plate are orthotropic and can be expressed as (Shen 2009)

$$E_{11} = V_F E_{11}^F + V_{MNC} E^{MNC} \tag{1}$$

$$\frac{1}{E_{22}} = \frac{1}{E_{22}^F} + \frac{V_{MNC}}{E^{MNC}} - V_F V_{MNC} - \frac{\frac{\nu_F^2 E^{MNC}}{E_{22}^F} + \frac{\nu_{MNC}^2 E_{22}^F}{E^{MNC}} - 2\nu^F \nu^{MNC}}{V_F E_{22}^F + V_{MNC} E^{MNC}} \tag{2}$$

$$\frac{1}{G_{12}} = \frac{V_F}{G_{12}^F} + \frac{V_{MNC}}{G^{MNC}} \tag{3}$$

$$\rho = V_F \rho^F + V_{MNC} \rho^{MNC} \tag{4}$$

$$\nu_{12} = V_F \nu^F + V_{MNC} \nu^{MNC} \tag{5}$$

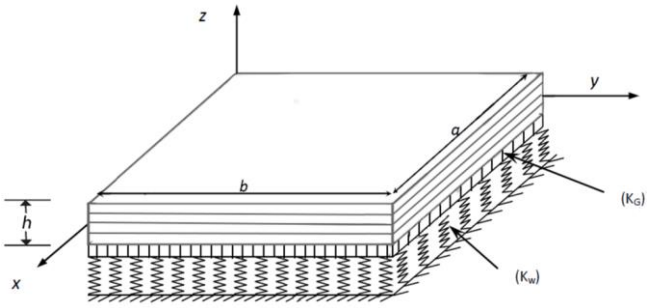

Fig. 1 The geometric parameters CNT reinforced multi-phase laminated composite plate resting on elastic foundations

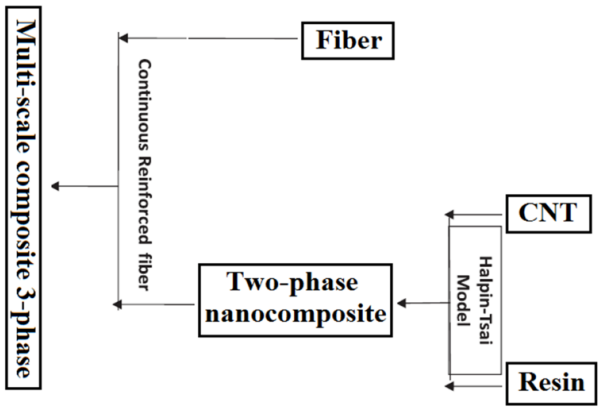

Fig. 2 Hierarchy of the CNT reinforced multi-phase laminated composite (Kim *et al.* 2009)

where E, G, ρ, V and ν denote the Young's modulus, shear modulus, mass density, volume fractions and Poisson's ratio, respectively, while the superscript or subscript F and MNC signify the fibers and matrix of nanocomposite, respectively.

Based on the Halpin-Tsai model, the tensile modulus of composites may be stated as (Kim *et al.* 2009)

$$E^{MNC} = \frac{E^M}{8}\left[5\left(\frac{1+2\beta_{dd}V_{CN}}{1-\beta_{dd}V_{CN}}\right) + 3\left(\frac{1+2(\ell^{CN}/d^{CN})\beta_{dl}V_{CN}}{1-\beta_{dl}V_{CN}}\right)\right] \tag{6}$$

$$\beta_{dl} = \frac{(E_{11}^{CN}/E^M)-(d^{CN}/4t^{CN})}{(E_{11}^{CN}/E^M)+(\ell^{CN}/2t^{CN})} \tag{7}$$

$$\beta_{dd} = \frac{(E_{11}^{CN}/E^M)-(d^{CN}/4t^{CN})}{(E_{11}^{CN}/E^M)+(d^{CN}/2t^{CN})} \tag{8}$$

where E^{CN}, t^{CN}, d^{CN}, ℓ^{CN} and V_{CN} indicate the Young's modulus, thickness, outer diameter, length and the volume fraction of carbon nanotubes, respectively, and E^M and V_M are the Young's modulus and volume fraction of the matrix, respectively.

The volume fraction of carbon nanotubes may be defined as (Rafiee *et al.* 2013)

$$V_{CN} = \frac{w_{CN}}{w_{CN}+\left(\frac{\rho^{CN}}{\rho^m}\right)-\left(\frac{\rho^{CN}}{\rho^m}\right)w_{CN}} \tag{9}$$

where w_{CN} is the mass fraction of the carbon nanotubes, ρ^m and ρ^{CN} are the mass densities of the matrix and carbon nanotube, respectively.

The Poisson's ratio and mass density ρ may be stated as

$$\nu^{MNC} = \nu^M \tag{10}$$

$$\rho^{MNC} = V_{CN}\rho^{CN} + V_M\rho^M \tag{11}$$

$$G^{MNC} = \frac{E^{MNC}}{2(1+\nu^{MNC})} \tag{12}$$

where ν^M is Poisson's ratio of the matrix. Since the amount of carbon nanotube was small, ν^{MNC} was considered to be the same as that of matrix (Kim *et al.* 2009, Rafiee *et al.* 2014b). The thermal expansion coefficients in the longitudinal and transverse directions can be expressed as (Shen 2009)

$$\alpha_{11} = \frac{V_F E_{11}^F \alpha_{11}^F + V_{MCN}E^{MCN}\alpha^{MCN}}{V_F E_{11}^F + V_{MCN}E^{MCN}} \tag{13}$$

$$\alpha_{22} = (1+\nu_{12}^F)V_F\alpha_{22}^F + (1+\nu^{MCN})V_{MCN}\alpha^{MCN} - \nu_{12}\alpha_{11} \tag{14}$$

where α_{11}^F and α_{22}^F are the thermal expansion coefficients of the fiber. α^{MCN} indicate the polymer matrix containing carbon nanotubes and is given by (Hu *et al.* 2013)

$$\alpha^{MCN} = \frac{1}{2}\{\left(\frac{V_{CN}E^{CN}\alpha^{CN}+V_M E^M\alpha^M}{V_{CN}E^{CN}+V_M E^M}\right)(1-\nu^{MNC}) + (1+\nu^M)\alpha^M V_M + (1+\nu^{CN})\alpha^{CN}V_{cn}\} \tag{15}$$

where α^{CN} and α^M are the thermal expansion coefficients of the carbon nanotube and epoxy resin matrix, respectively. The temperature distributions are assumed through the thickness of the plate by Na and Kim (2004)

$$T(z) = T_0 + \Delta T \quad \text{Uniform} \tag{16}$$

$$T(z) = T_0 + \Delta T\left(\frac{z}{h}\right) \quad \text{Linear} \tag{17}$$

$$T(z) = T_0 + \Delta T\left(\frac{\Theta(z)}{h}\right) \quad \text{Nonlinear} \tag{18}$$

where ΔT is the rise in temperature with respect to T_0 the reference temperature, respectively.

2.2 Displacement field model

According to the Inverse Hyperbolic Shear Deformation Theory, the displacement field of laminated plate theory can be expressed as (Grover *et al.* 2013)

$$u(x,y,z,t) = u_0(x,y,t) - z\frac{\partial w_0}{\partial x} + \Theta(z)\phi_x(x,y,t)$$
$$v(x,y,z,t) = v_0(x,y,t) - z\frac{\partial w_0}{\partial y} + \Theta(z)\phi_y(x,y,t) \tag{19}$$
$$w(x,y,z,t) = w_0(x,y,t)$$

where u_0, v_0, and w_0 denote the displacements at the mid-plane of the reference plane of the plate and ϕ_x and ϕ_y are rotations about the y and x axes, respectively.

$\Theta(z)$ indicate the transverse shear function and is given by (Grover *et al*. 2013)

$$\Theta(z) = cot^{-1}\left(\frac{rh}{z}\right) - \frac{4rz}{[h(4r^2+1)]}\,; r = 0.46 \quad (20)$$

The strain–displacement relations, based on von Kármán's large deformation assumption are (Ebrahimi and Habibi 2016)

$$\begin{Bmatrix}\varepsilon_{xx}\\ \varepsilon_{yy}\\ \gamma_{xy}\end{Bmatrix} = \varepsilon_0 + z\varepsilon_1 + \Theta(z)\varepsilon_3\,, \begin{Bmatrix}\gamma_{yz}\\ \gamma_{xz}\end{Bmatrix} = \gamma_0 + \frac{\partial\Theta(z)}{\partial \mathrm{z}}\gamma_1 \quad (21)$$

where

$$\varepsilon_0 = \begin{Bmatrix} \frac{\partial u_0}{\partial \mathrm{x}} + \frac{1}{2}\left(\frac{\partial w_0}{\partial x}\right)^2 \\ \frac{\partial v_0}{\partial \mathrm{y}} + \frac{1}{2}\left(\frac{\partial w_0}{\partial y}\right)^2 \\ \frac{\partial u_0}{\partial \mathrm{y}} + \frac{\partial v_0}{\partial \mathrm{x}} + \frac{\partial w_0}{\partial x}\frac{\partial w_0}{\partial y} \end{Bmatrix}, \varepsilon_1 = \begin{Bmatrix} \frac{\partial \phi_x}{\partial \mathrm{x}} \\ \frac{\partial \phi_y}{\partial \mathrm{y}} \\ \frac{\partial \phi_x}{\partial \mathrm{y}} + \frac{\partial \phi_y}{\partial \mathrm{x}} \end{Bmatrix},$$
$$\varepsilon_2 = \begin{Bmatrix} \frac{\partial \phi_x}{\partial \mathrm{x}} + \frac{\partial^2 w_0}{\partial x^2} \\ \frac{\partial \phi_y}{\partial \mathrm{y}} + \frac{\partial^2 w_0}{\partial y^2} \\ \frac{\partial \phi_x}{\partial \mathrm{y}} + \frac{\partial \phi_y}{\partial \mathrm{x}} + 2\frac{\partial^2 w_0}{\partial x \partial y} \end{Bmatrix}, \gamma_0 = \begin{Bmatrix} \frac{\partial w_0}{\partial x} + \phi_x \\ \frac{\partial w_0}{\partial y} + \phi_y \end{Bmatrix}, \quad (22)$$
$$\gamma_1 = \begin{Bmatrix} \frac{\partial w_0}{\partial x} + \phi_x \\ \frac{\partial w_0}{\partial y} + \phi_y \end{Bmatrix}$$

In the above relations, ε_{xx}, ε_{yy} and γ_{xy} denote in-plane strains. Also, γ_{yz} and γ_{xz} are transverse shear strains. The governing equations can be generated by applying principle of virtual work (Lei *et al*. 2014)

$$\int_{-\frac{h}{2}}^{\frac{h}{2}}\int_0^{\mathrm{b}}\int_0^{\mathrm{a}} \{\delta\varepsilon\}^{\mathrm{T}}\{\sigma\} dxdydz + \int_{-\frac{h}{2}}^{\frac{h}{2}}\int_0^{\mathrm{b}}\int_0^{\mathrm{a}} \rho(\ddot{u}\delta u + \ddot{v}\delta v + \ddot{w}\delta w)\, dxdydz - \int_0^{\mathrm{b}}\int_0^{\mathrm{a}} q_e \delta w\, dxdy - f(t)\delta\alpha = 0 \quad (23)$$

where q_e denote the density of reaction force of foundation and is given by (Chien and Chen 2006)

$$q_e = K_1 w - K_2\left(\frac{\partial^2 w}{\partial x^2} + \frac{\partial^2 w}{\partial y^2}\right) \quad (24)$$

where K_1 and K_2 are stiffness of Winkler's and Pasternak foundation. $f(t)$ is the impulsive load and can be any one of the types is given by (Shen *et al*. 2000)

$$f(t) = f_0 \quad \text{Sudden} \quad (25)$$

$$f(t) = \begin{cases} f_0\,, t \le t_0 \\ 0\,, t_0 \le t \end{cases} \quad \text{Step} \quad (26)$$

$$f(t) = \begin{cases} f_0\left(1 - \frac{t}{t_0}\right), t \le t_0 \\ 0\,, \quad t_0 \le t \end{cases} \quad \text{Triangular} \quad (27)$$

$$f(t) = \begin{cases} f_0\left(1 - \frac{t}{t_0}\right), t \le t_0 \\ 0\,, \quad t_0 \le t \end{cases} \quad \text{Half-sine} \quad (28)$$

$$f(t) = f_0 e^{-\tau t} \quad \text{Exponential} \quad (29)$$

2.3 Constitutive equations

The constitutive relation of the *k*th layer of the laminate in the material axes can be stated as (Reddy 2004)

$$\begin{Bmatrix}\sigma_1\\ \sigma_2\\ \tau_{23}\\ \tau_{31}\\ \tau_{12}\end{Bmatrix} = \begin{bmatrix} Q_{11} & Q_{12} & 0 & 0 & 0 \\ Q_{12} & Q_{22} & 0 & 0 & 0 \\ 0 & 0 & Q_{44} & 0 & 0 \\ 0 & 0 & 0 & Q_{55} & 0 \\ 0 & 0 & 0 & 0 & Q_{66} \end{bmatrix} \left(\begin{Bmatrix}\varepsilon_1\\ \varepsilon_2\\ \gamma_{23}\\ \gamma_{31}\\ \gamma_{12}\end{Bmatrix} - \begin{Bmatrix}\alpha_{11}\\ \alpha_{22}\\ 0\\ 0\\ 0\end{Bmatrix} (T(z) - T_0) \right) \quad (30)$$

where

$$Q_{11} = \frac{E_{11}}{1 - \nu_{12}\nu_{21}},$$
$$Q_{66} = G_{12}\,, Q_{22} = \frac{E_{22}}{1 - \nu_{12}\nu_{21}}\,,\; Q_{44} = G_{23} \quad (31)$$
$$Q_{12} = \frac{\upsilon_{12}E_{22}}{1 - \nu_{12}\nu_{21}}\,,\; Q_{55} = G_{13}$$

If the fiber angle with the geometric x axis is denoted by θ, the relation (30) can be transferred to the geometric coordinates as

$$\begin{Bmatrix}\sigma_{\mathrm{x}}\\ \sigma_{\mathrm{y}}\\ \tau_{\mathrm{yz}}\\ \tau_{\mathrm{xz}}\\ \tau_{\mathrm{xy}}\end{Bmatrix}_{\mathrm{k}} = \begin{bmatrix} \overline{Q}_{11} & \overline{Q}_{12} & 0 & 0 & \overline{Q}_{16} \\ \overline{Q}_{12} & \overline{Q}_{22} & 0 & 0 & \overline{Q}_{26} \\ 0 & 0 & \overline{Q}_{44} & \overline{Q}_{45} & 0 \\ 0 & 0 & \overline{Q}_{45} & \overline{Q}_{55} & 0 \\ \overline{Q}_{16} & \overline{Q}_{26} & 0 & 0 & \overline{Q}_{66} \end{bmatrix}_{\mathrm{k}} \left(\begin{Bmatrix}\varepsilon_{\mathrm{x}}\\ \varepsilon_{\mathrm{y}}\\ \gamma_{\mathrm{yz}}\\ \gamma_{\mathrm{xz}}\\ \gamma_{\mathrm{xy}}\end{Bmatrix} - \begin{Bmatrix}\alpha_{11}\\ \alpha_{22}\\ 0\\ 0\\ 0\end{Bmatrix} (T(z) - T_0) \right)_{\mathrm{k}} \quad (32)$$

where

$$\overline{Q}_{11} = Q_{11}cos^4\theta + 2(Q_{12} + 2Q_{66})sin^2\theta cos^2\theta + Q_{22}sin^4\theta$$
$$\overline{Q}_{12} = (Q_{11} + Q_{22} - 4Q_{66})sin^2\theta cos^2\theta + Q_{12}(sin^4\theta + cos^4\theta)$$
$$\overline{Q}_{22} = Q_{11}sin^4\theta + 2(Q_{12} + 2Q_{66})sin^2\theta cos^2\theta + Q_{22}cos^4\theta$$
$$\overline{Q}_{16} = (Q_{11} - Q_{12} - 2Q_{66})sin\theta cos^3\theta + (Q_{12} - Q_{22} + 2Q_{66})sin^3\theta cos\theta$$
$$\overline{Q}_{26} = (Q_{11} - Q_{12} - 2Q_{66})sin^3\theta cos\theta + (Q_{12} - Q_{22} + 2Q_{66})sin\theta cos^3\theta$$
$$\overline{Q}_{66} = (Q_{11} + Q_{22} - 2Q_{12} - 2Q_{66})sin^2\theta cos^2\theta + Q_{66}(sin^4\theta + cos^4\theta)$$
$$\overline{Q}_{44} = Q_{44}cos^2\theta + Q_{55}sin^2\theta$$

$$\overline{Q}_{45} = (Q_{55} - Q_{44})cos\theta sin\theta$$
$$\overline{Q}_{55} = Q_{55}cos^2\theta + Q_{44}sin^2\theta \quad (33)$$

3. Finite element formulation

There are also nonlinearities in the realistic mechanical problems which generate difficulties in the solving procedure of the final governing equations of these problems. Based on this phenomenon, it is usually hard or sometimes impossible to solve nonlinear problems incorporating analytical solution methods. In this cases, researchers majorly prefer to choose powerful numerical solution methods like differential transformation method (DTM), differential quadrature method (DQM), discrete singular convolution method (DSCM), finite element method (FEM) and so on instead of analytical ones. Baltacıoglu *et al*. (2010) developed a DSC based model in order to solve the nonlinear bending characteristics of composite plates. Later, Tornabene *et al*. (2015) combined the FEM with the DQM and presented that these methods are powerful enough for the goal of solving mechanical problems. Ebrahimi *et al*. (2015) showed the accuracy of the DTM for solving the vibrational responses of compositionally graded nanobeams.

In present section, the equations of CNT reinforced multi-phase laminated composite plate by applying finite element method are discretized. Based on Eq. (23), one may write (Ebrahimi and Habibi 2016)

$$\begin{aligned}&\left\{\int_{-h/2}^{h/2}\int_{\Omega_0} \delta {D_0}^t(\iota_0 + z\iota_1 + \Theta(z)\iota_2 + \iota_N)^t \right.\\ &Q_p\left(\iota_0 + z\iota_1 + \Theta(z)\iota_2 + (\frac{1}{2})\iota_N\right)D_0\\ &+\delta {D_0}^t\left(\iota_{s0} + \frac{\partial\Theta(z)}{\partial z}\iota_{s1}\right)^t Q_s\left(\iota_{s0} + \frac{\partial\Theta(z)}{\partial z}\iota_{s1}\right)D_0\\ &\left.+\delta {D_0}^t\rho(\iota_{\theta 0} + z\iota_{\theta 1} + \Theta(z)\iota_{\theta 2})^t\,(\iota_{\theta 0} + z\iota_{\theta 1} + \Theta(z)\iota_{\theta 2})D_0\right\}\\ &d\Omega dz - \int_{\Omega_0}\delta {D_0}^t q^{Th}\,d\Omega dz - \delta {D_0}^t(f(t) - q_e) = 0\end{aligned} \quad (34)$$

where $\{D_0\} = \{u_0, v_0, w_0, \phi_x, \phi_y\}^t$ is the displacement vector of a point in middle-plane, and

$$Q_p = \begin{bmatrix}\overline{Q}_{11} & \overline{Q}_{12} & \overline{Q}_{16}\\ \overline{Q}_{12} & \overline{Q}_{22} & \overline{Q}_{26}\\ \overline{Q}_{16} & \overline{Q}_{26} & \overline{Q}_{66}\end{bmatrix}, Q_s = \begin{bmatrix}\overline{Q}_{44} & \overline{Q}_{45}\\ \overline{Q}_{45} & \overline{Q}_{55}\end{bmatrix} \quad (35)$$

$$\iota_0 = \begin{bmatrix}\frac{\partial}{\partial x} & 0 & 0 & 0 & 0\\ 0 & \frac{\partial}{\partial y} & 0 & 0 & 0\\ \frac{\partial}{\partial y} & \frac{\partial}{\partial x} & 0 & 0 & 0\end{bmatrix}, \iota_1 = \begin{bmatrix}0 & 0 & 0 & \frac{\partial}{\partial x} & 0\\ 0 & 0 & 0 & 0 & \frac{\partial}{\partial y}\\ 0 & 0 & 0 & \frac{\partial}{\partial y} & \frac{\partial}{\partial x}\end{bmatrix},$$

$$\iota_2 = \begin{bmatrix}0 & 0 & \frac{\partial^2}{\partial x^2} & \frac{\partial}{\partial x} & 0\\ 0 & 0 & \frac{\partial^2}{\partial y^2} & 0 & \frac{\partial}{\partial y}\\ 0 & 0 & 2\frac{\partial}{\partial y}\frac{\partial}{\partial x} & \frac{\partial}{\partial y} & \frac{\partial}{\partial x}\end{bmatrix}, \iota_{s0} = \begin{bmatrix}0 & 0 & \frac{\partial}{\partial x} & 0 & 1\\ 0 & 0 & \frac{\partial}{\partial y} & 1 & 0\end{bmatrix}$$

$$\iota_{s1} = \begin{bmatrix}0 & 0 & \frac{\partial}{\partial x} & 0 & 1\\ 0 & 0 & \frac{\partial}{\partial y} & 1 & 0\end{bmatrix}, \iota_{\theta 0} = \begin{bmatrix}1 & 0 & 0 & 0 & 0\\ 0 & 1 & 0 & 0 & 0\\ 0 & 0 & 1 & 0 & 0\end{bmatrix},$$

$$\iota_{\theta 1} = \begin{bmatrix}0 & 0 & 0 & 1 & 0\\ 0 & 0 & 0 & 0 & 1\\ 1 & 0 & 0 & 0 & 0\end{bmatrix}, \iota_{\theta 2} = \begin{bmatrix}0 & 0 & \frac{\partial}{\partial x} & 1 & 0\\ 0 & 0 & \frac{\partial}{\partial y} & 0 & 1\\ 0 & 0 & 0 & 0 & 0\end{bmatrix}, \quad (36)$$

$$\iota_N = \begin{bmatrix}0 & 0 & \frac{\partial w_0}{\partial x}\frac{\partial}{\partial x} & 0 & 0\\ 0 & 0 & \frac{\partial w_0}{\partial y}\frac{\partial}{\partial y} & 0 & 0\\ 0 & 0 & \frac{\partial w_0}{\partial x}\frac{\partial}{\partial y} + \frac{\partial w_0}{\partial y}\frac{\partial}{\partial x} & 0 & 0\end{bmatrix}$$

and q^{Th} denote the thermal force and is given by

$$q^{Th} = (\iota_0 + z\iota_1 + z^3\iota_3)^t Q_p \begin{Bmatrix}\alpha_{11}\\ \alpha_{22}\\ 0\end{Bmatrix}(T(z) - T_0) \quad (37)$$

From the strain-displacement relationships, can observe that the first and second-order derivatives of generalized displacements are appeared in equations. Therefore, to guarantee the integrability of equations, the C^1-continuity of the generalized displacement functions is generally necessary in finite element procedure (Ebrahimi and Habibi 2016). Hence, in this paper, the four-nodded rectangular conforming element based on HSDT is used. The element is C^1-continuous via 15 DOF at each node**.** According to the nodal displacement vector, the displacement vector of the reference plane may be written as

$$\boldsymbol{D_0}^{(e)} = \begin{pmatrix}\psi_1 & \dots & 0 & & \psi_{4y} & \dots & 0\\ 0 & & 0 & & 0 & & 0\\ 0 & \ddots & 0 & \dots & 0 & \ddots & 0\\ 0 & & 0 & & 0 & & 0\\ 0 & \dots & \psi_1 & & 0 & \dots & \psi_{4y}\end{pmatrix}_{5\times 60}$$
$$\{d^e\} = \psi {d_0}^{(e)} \quad (38)$$

where:

$$\{d^e\} = \begin{Bmatrix}u_{0i}, v_{0i}, w_{0i}, \phi_{xi}, \phi_{yi}, u_{0i,x}, v_{0i,x}, w_{i,x},\\ \phi_{xi,x}, \phi_{yi,x}, u_{0i,y}, v_{0i,y}, w_{0i,y}, \phi_{xi,y}, \phi_{yi,y}\end{Bmatrix}^T$$ are the 15-DOF associated with each node.

The displacement interpolation functions can be written as

$$\psi_i = \frac{1}{8}(1 + \xi_i\xi)(1 + \eta_i\eta)(2 + \xi_i\xi + \eta_i\eta - \xi^2 - \eta^2), \quad (39)$$

$$\psi_{ix} = \frac{1}{8}a\xi_i(1 + \xi_i\xi)^2(1 + \eta_i\eta)(\xi_i\xi - 1), \quad (40)$$

$$\psi_{iy} = \frac{1}{8}b\eta_i(1 + \xi_i\xi)(\eta_i\eta - 1)(1 + \eta_i\eta)^2, \quad (41)$$

where α and β are the half length of element in the x and y directions and the normalized coordinates are

$$\xi = \frac{x - x_c}{a}.\ \ \eta = \frac{y - y_c}{b} \quad (42)$$

where (x_c, y_c) is the center of rectangular element. Based on Eqs. (38)-(42), Eq. (34) can be expressed as

$$\left(\delta d^{(e)}\right)^t \left\{\int\int_{\Omega_0}\left[\begin{array}{l}\sum_{i=0}^{2} B_i{}^t\left(Q_i^{(e)}B_0+Q_{i+1}^{(e)}B_1+Q_{i+2}^{(e)}B_2\right)d^{(e)}+\\ +\sum_{i=0}^{1} B_{si}{}^t\left(Q_{s(i)}^{(e)}B_{s0}+Q_{s(i+1)}^{(e)}B_{s1}\right)d^{(e)}\\ +\sum_{i=0}^{2} B_{\theta i}{}^t\left(I_i^{(e)}B_{\theta 0}+I_{i+1}^{(e)}B_{\theta 1}+I_{i+2}^{(e)}B_{\theta 2}\right)d^{(e)}-\\ [B_0^t\ B_1^t\ B_3^t]\begin{bmatrix}q_0^{Th}\\ q_1^{Th}\\ q_3^{Th}\end{bmatrix}\end{array}\right] d\Omega-\psi^t(f(t)-q_e)^{(e)}\right\}=0 \quad (43)$$

where

$$(q_0^{Th},q_1^{Th},q_2^{Th}) = \int_{-\frac{h}{2}}^{\frac{h}{2}}\begin{bmatrix}\overline{Q}_{11}\alpha_{11}+\overline{Q}_{12}\alpha_{22}\\ \overline{Q}_{12}\alpha_{22}+\overline{Q}_{22}\alpha_{11}\\ \overline{Q}_{16}\alpha_{11}+\overline{Q}_{26}\alpha_{11}\end{bmatrix}(1,z,\Theta(z))(\mathrm{T}(z)-T_0)\mathrm{d}z \quad (44)$$

$$(B_0,B_1,B_2,B_N,B_{s0},B_{s1},B_{\theta 0},B_{\theta 1},B_{\theta 2}) = (\iota_0,\iota_1,\iota_2,\iota_N,\iota_{s0},\iota_{s1},\iota_{\theta 0},\iota_{\theta 1})\psi$$

$$(Q_0,Q_1,Q_2,Q_3,Q_4,Q_5) = \int_{-\frac{h}{2}}^{\frac{h}{2}} Q_p(1,z,\Theta(z),z^2,z\Theta(z),\Theta^2(z))dz$$

$$(Q_{s0},Q_{s1},Q_{s2}) = \int_{-\frac{h}{2}}^{\frac{h}{2}} Q_s(1,(\frac{\partial\Theta(z)}{\partial z}),(\frac{\partial\Theta(z)}{\partial z})^2)dz \quad (45)$$

$$(I_0,I_1,I_2,I_3,I_4,I_5) = \int_{-\frac{h}{2}}^{\frac{h}{2}} \rho(1,z,\Theta(z),z^2,z\Theta(z),\Theta^2(z))dz$$

Eq. (45) holds for any arbitrary $\left(\delta d^{(e)}\right)^t \neq 0$, therefore in a compact form

$$K_L^{(e)}d_0^{(e)}+K_{NL}^{(e)}d_0^{(e)}+M^{(e)}\ddot{d}_0^{(e)}=F^{(e)} \quad (46)$$

where, the element stiffness matrixes $K_L^{(e)}$, $K_{NL}^{(e)}$, element load vector $F^{(e)}$, element mass matrix $M^{(e)}$ and can be given as

$$K^{(e)}=K_L^{(e)}+K_{NL}^{(e)} = \int_{\Omega_0}\left[\sum_{i=0}^{2} B_i{}^t\left(Q_i^{(e)}B_0+Q_{i+1}^{(e)}B_1+Q_{i+2}^{(e)}B_2\right)+\sum_{i=0}^{1} B_{si}{}^t\left(Q_{si}^{(e)}B_{s0}+Q_{s(i+1)}^{(e)}B_{s1}\right)\right]dxdy + B_N{}^t\left(Q_0^{(e)}B_0+Q_1^{(e)}B_1+Q_2^{(e)}B_2+\left(\frac{1}{2}\right)Q_0^{(e)}B_N\right)+\left(\frac{1}{2}\right)(B_0+B_1+B_2)Q_0^{(e)}B_N \quad (47)$$

$$F^{(e)}=Y^{(e)}+\psi^t(f(t)-q_e)^{(e)} \quad (48)$$

$$M^{(e)} = \int_{\Omega_0}\left[\sum_{i=0}^{2} B_{\theta i}{}^t\left(I_i^{(e)}B_{\theta 0}+I_{i+1}^{(e)}B_{\theta 1}+I_{i+2}^{(e)}B_{\theta 2}\right)\right]dxdy \quad (49)$$

where $Y^{(e)}$ is the element force vector due to thermal

$$Y^{(e)}=\int_{\Omega_0^{(e)}}[B_0^t\ B_1^t\ B_3^t]\begin{bmatrix}q_0^{Th}\\ q_1^{Th}\\ q_3^{Th}\end{bmatrix}dxdy \quad (50)$$

Resulting time-dependent may be expressed as

$$[K]\{d\}+[M]\{\ddot{d}\}=\{F\} \quad (51)$$

where, d and $\ddot{d}$ are respectively the displacement and acceleration vector. F is the global load vector, which includes the impact force and thermal force K is the global stiffness matrix, includes linear and nonlinear stiffness matrix. Also M denote the global mass matrix.

The boundary conditions for clamped and simply supported conditions are given below:

$u_n = u_s = w_0 = \phi_n = \phi_s = 0$ (Clamped edge)

$u_s = w_0 = \phi_s = 0$ (Simply supported edge)

where the subscripts s and n denote the tangential and normal directions, respectively, on the boundaries.

Table 1 Material properties of the multi-phase nanocomposite plate (Zhang and Wang 2006, Rafiee *et al.* 2014b)

Material properties of fiber (carbon):	
E_{11}^F=233.05 GPa, E_{22}^F=23.1 GPa , G_{12}^F =8.96 GPa, ν^F=0.2 , ρ^F=1750 kg/m , V_F =0.6	
$\alpha_{11}=-0.54\times10^{-6}\,K^{-1}$, α_{22} =10.08 $\times10^{-6}\,K^{-1}$	
Material properties of epoxy matrix:	
ν^M=0.34, ρ^M=1150 kg/m3 , E^M=2.5 GPa	
$\alpha=45\times10^{-6}\,K^{-1}$	
$\beta=2.68\times10^{-3}$ wt%$^{-1}$	
Material properties of CNT:	
SWCNT:	MWCNT:
E^{CN}=640 GPa	E^{CN}=400 GPa
d^{CN} =1.4× 10^{-9} m	d^{CN} =20× 10^{-9} m
t^{CN}=0.34× 10^{-9} m	t^{CN}=0.34× 10^{-9} m
ρ^{CN}=1350 kg/m^3	ρ^{CN}=1350 kg/m^3
ν_{12}^{CN}=0.33	ν_{12}^{CN}=0.33
ℓ^{CN} =25× 10^{-6} m	ℓ^{CN} =50× 10^{-6} m
α =3.4584× $10^{-6}\,K^{-1}$	

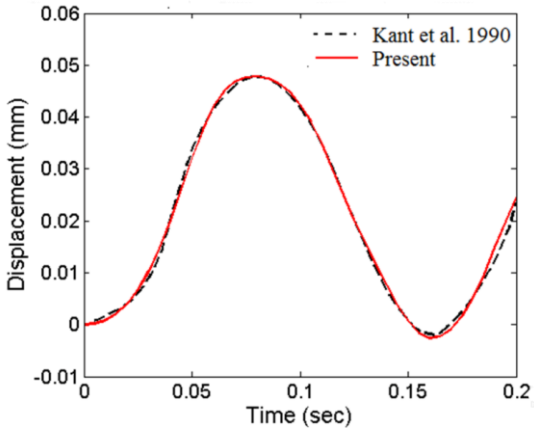

Fig. 3 Comparisons of central deflection history of an (CFRC) composite laminated plate subjected to suddenly applied uniform load

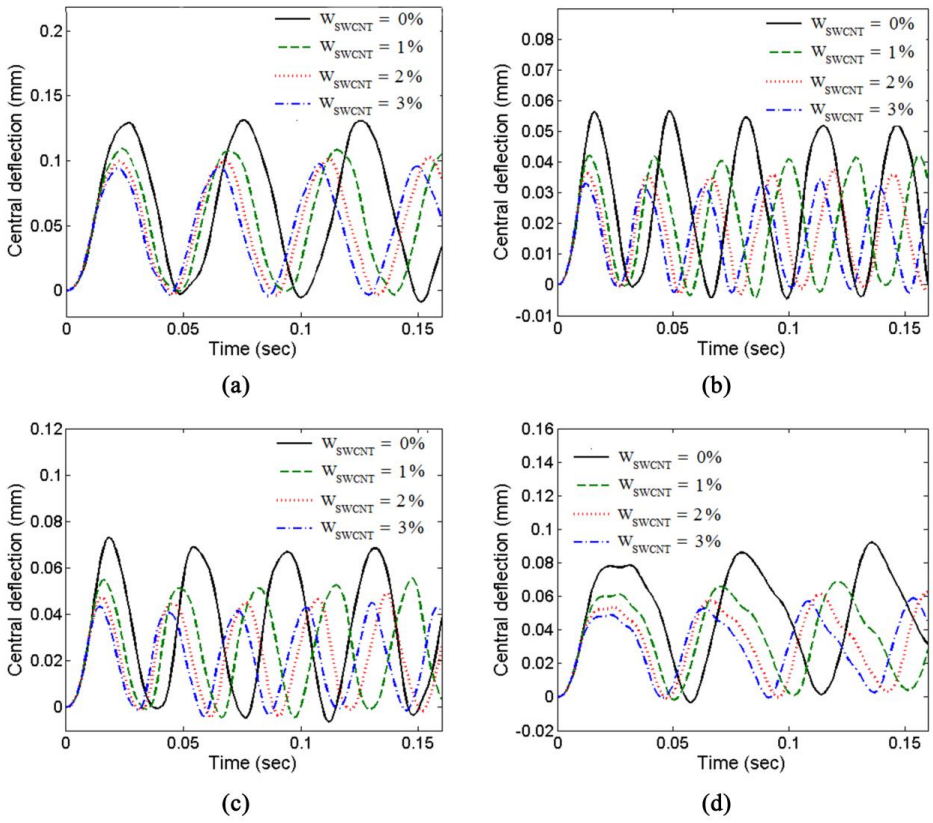

Fig. 4 Effect of the weight percentage of SWCNTs on the central deflection of plate (ΔT=0 K) (a) SSSS; (b) CCCC; (c) CSCS, (d) CCCF

In order to solve Eq. (53), Newmark's numerical time integration method is used. Based on this method, accelerations and velocities of the end of each time step are computed by Zhu *et al*. (2005)

$$\ddot{\Lambda}_{j+1} = a_1\left(\Lambda_{j+1} - \Lambda_j\right) - a_2\dot{\Lambda}_j - a_3\ddot{\Lambda}_j$$
$$\dot{\Lambda}_{j+1} = \dot{\Lambda}_j + a_4\ddot{\Lambda}_j + a_5\ddot{\Lambda}_j \tag{52}$$

where j is the time step counter and

$$a_1 = \frac{2}{\zeta(\Delta t)^2};\ a_2 = \frac{2}{\zeta\Delta t};\ a_3 = \frac{1}{\zeta} - 1;\ \zeta \le \lambda$$
$$a_4 = \Delta t(1-\lambda);\ a_5 = \lambda\Delta t;\ \lambda \ge 0.5 \tag{53}$$

By substituting Eq. (52) into Eq. (51), we obtain

$$\hat{K}_{j+1}\Lambda_{j+1} = \hat{F}_{j+1} \tag{54}$$

where

$$\hat{K}_{j+1} = K_{j+1} + a_1 M_{j+1} \tag{55}$$

$$\hat{F}_{j+1} = H_j M_{j+1} + F_j \tag{56}$$

where H_j is the following vector

$$H_j = a_1\Lambda_i + a_2\dot{\Lambda}_i - a_3\ddot{\Lambda}_j \tag{57}$$

Since Eq. (51) is a nonlinear equation, Picard or Newton-Raphson method has to be employed in each time step to reach a convergence criterion, e.g.

$$\frac{\left\|\Lambda_i{}^{(\eta+1)} - \Lambda_i{}^{(\eta)}\right\|}{\Lambda_i{}^{(\eta+1)}} \cong \Delta \tag{58}$$

where j, η and Δ are the time step counter, iteration counter, and a sufficiently small number, respectively.

3. Results and discussions

In present section, after examining the validity of the present work, the effects of the weight percentage of SWCNTs and MWCNTs, nanotube aspect ratio, volume fraction of fibers, plate aspect, temperature, elastic foundation parameters, distribution of temperature and shape of impulsive on nonlinear dynamic response of CNT reinforced multi-phase laminated composite plate are studied in details. Due to enable tracing time variations of the response more adequately, the time integration steps must be much less than the fundamental natural period of the structure. Hence in this paper, a time step that is equal or less than 10^{-6} (sec) is chosen. Also $\Delta = 0.0001$ is used for the convergence criterion (Eq. (51)).

3.1 Validation

To validate the results of the present work, an example previously used by Kant *et al.* (1990) is re-solved. The material properties and geometrical parameters are set according to that in (Kant *et al.* 1990), of which the results are compared. Material properties of the [0/90/90/0] composite plate are E_1/E_2=25, E_2=2.1×10^{-6} N/cm^2; G_{12}= G_{13}=G_{23}=0.5E_2; G_{12}=3.5 GPa; ν_{12}=0.25; ρ=8×10^{-6} N.s^2/cm^4. The plate is simply supported with geometrical properties

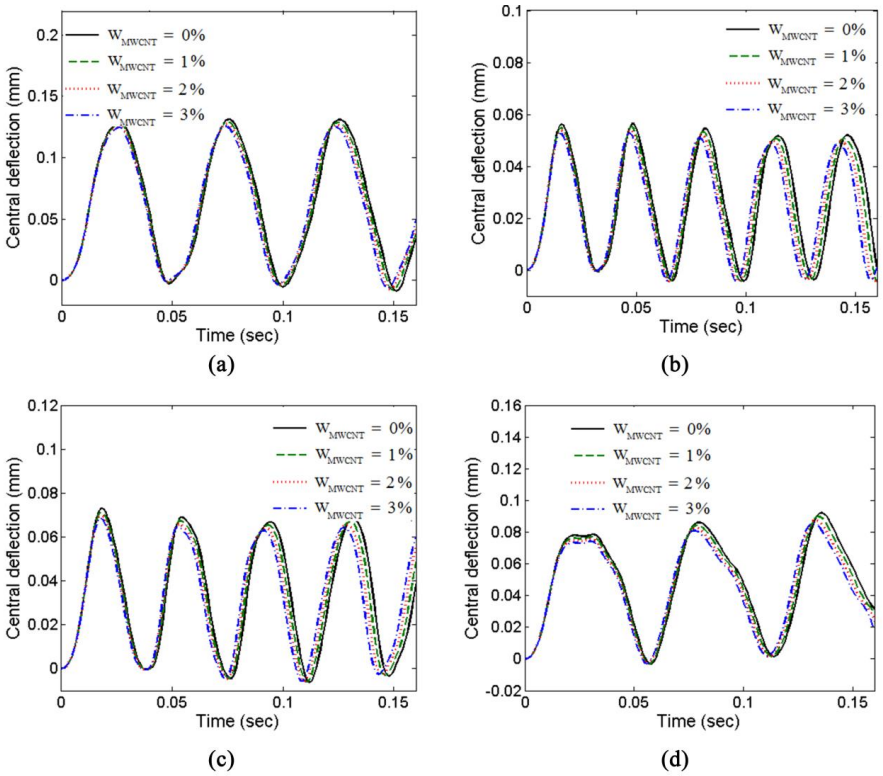

Fig. 5 Effect of the weight percentage of MWCNTs on the central deflection of plate (ΔT= 0 K). (a) SSSS; (b) CCCC; (c) CSCS, (d) CCCF

a=b=25 mm and h=5 cm. The suddenly applied uniform load has f_0=10 N/cm^2. In Fig. 3 the results of this study for the central deflection histories are compared with those presented by Kant *et al.* (1990). As it is obvious from Fig. 3, there is a good agreement between present results and results of Kant *et al*.

3.2 Parametric studies

In this section, nonlinear dynamic response of polymer/CNT/fiber multiphase nanocomposite plate resting on elastic foundations in thermal environments investigated. A plate with material properties listed in the Table 1 and geometry a=b=200 mm and h=20 mm and the stacking sequence [0/90/90/0] is considered. The dynamic load is assumed to be a suddenly applied uniform load with f_0=2 MPa. Volume fraction of fibers V^F=0.7 is considered. For convenience, dimensionless foundation stiffness is defined by:

$$D_0 = \frac{E_o h^3}{12(1-\nu_0^2)}, K_w = \frac{K_1 b^4}{D_0}, K_s = \frac{K_2 b^2}{D_0}$$

3.2.1 Effect of adding CNT

Effect of weight percentage of CNT on the nonlinear dynamic response of a multi-phase laminated composite plate reinforced with SWCNT and MWCNT under different boundary conditions are depicted in Fig. 3, Fig. 4. Four different weight percentage of carbon nanotube, w_{CN}=0%, 1%, 2% and 3% are considered. Four sets of boundary conditions, i.e., CCCC, SSSS, CCCF and CSCS, are considered. As may be noted, Increasing the CNTs weight percentage leads to a plate with higher bending rigidity and subsequently, higher natural frequencies and smaller response times. Due to this reason, central deflection has decreased with increasing the weight percentage. Further the effect of weight percentage of is more prominent in SWCNTs reinforced composite plates rather than MWCNTs reinforced composite plates.

Also, as can be observed, The central deflection related to the CCCC boundary is the lowest, followed by CCCF, CSCS and SSSS in that order.

Fig. 5 show the effect of aspect ratio of CNT on the nonlinear dynamic response of simply supported, symmetric cross ply, SWCNT and MSCNT reinforced multi-phase laminated composite plate. Four sets of aspect ratios have been considered here, i.e., ℓ^{CN}/d^{CN}=100; 500; 1000, and 2000.

As may be noted, composite plate reinforced with longer CNTs has more stiffening behavior and as the aspect ratio of CNT increases the peaks of central deflection decreases. It should be noted that for aspect ratios higher than 500 (ℓ^{CN}/d^{CN}>500) this effect insignificant.

3.2.2 Effect of thermal environment

In this section, it is intended to investigate effect of thermal environment on the nonlinear dynamic response of a multi-phase laminated composite plate reinforced with single walled carbon nanotube. In this regard, weight percentage of SWCNT w_{cn}=3% is considered. The temperature field is assumed to be varied uniformly through the thickness of the plate. Specifications are the same with the preceding section.

Table 2 Effect of temperature rise and volume fraction of fibers on the central deflection (10^{-5} m) for simply supported CNT reinforced multi-phase laminated composite plate with different SWCNTs weight percentage

ℓ^{CN}/d^{CN}	w_{cn}	ΔT=0 [K]			ΔT=100 [K]			ΔT=200 [K]		
		V_F			V_F			V_F		
		0.6	0.7	0.8	0.6	0.7	0.8	0.6	0.7	0.8
100	0	15.3957	12.9177	10.7348	17.1322	14.4282	12.0757	18.8687	15.9386	13.4166
	1	13.8950	11.7734	9.91972	15.9384	13.5083	11.4112	17.9818	15.2432	12.9141
	2	12.8871	11.0236	9.40035	15.1758	12.9420	11.0232	17.4671	14.8603	12.6460
	3	12.1691	10.4771	9.03984	14.6656	12.5405	10.7543	17.1622	14.6038	12.4687
500	0	15.3957	12.9177	10.7348	17.1322	14.4282	12.0757	18.8687	15.9386	13.4166
	1	13.1253	11.1857	9.52336	15.3646	13.0627	11.1209	17.6039	14.9397	12.7184
	2	11.9065	10.2848	8.90396	14.5008	12.4293	10.6699	17.0950	14.5738	12.4359
	3	11.1138	9.70095	8.51021	13.9972	12.0425	10.3927	16.8978	14.3890	12.2870
1000	0	15.3957	12.9177	10.7348	17.1322	14.4282	12.0757	18.8687	15.9386	13.4166
	1	12.9530	11.0698	9.43509	15.2390	12.9833	11.0553	17.525	14.8968	12.6756
	2	11.7197	10.1429	8.80562	14.3873	12.3387	10.6040	17.0549	14.5346	12.4024
	3	10.9259	9.56605	8.42291	13.9013	11.9703	10.3437	16.8767	14.3745	12.2645

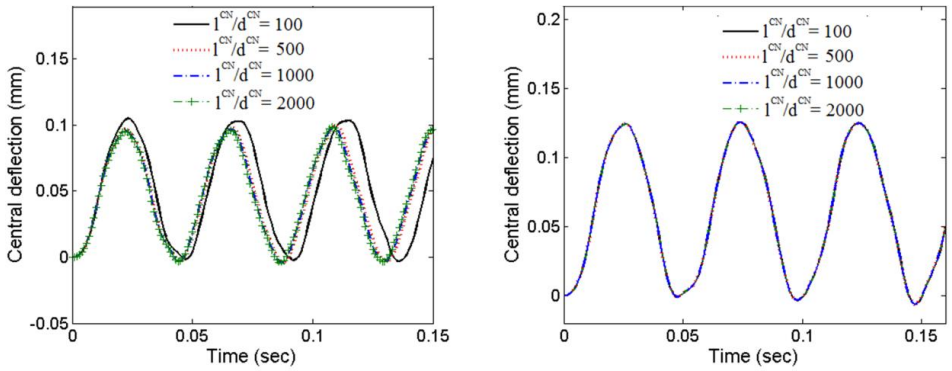

Fig. 6 Effect of the of CNTs aspect ratio on the central deflection of plate (ΔT= 0 K) .(a) SWCNT; (b) MWCNT

Table 2 present the effect of temperature rise and volume fraction of fibers on the maximum deflection for simply supported CNT reinforced multi-phase laminated composite plate with different SWCNTs weight percentage. As may be observed, as the plate temperature increases peak central deflection increases. That is because increasing the plate temperature leads to structure loses stiffness generally.

As mentioned in Fig. 3 and Fig. 4 central deflection of plate has decreased with increasing the weight percentage, but From Table 1, it is noticed that in thermal environment central deflection of plate was reduced using a maximum of 1% of the CNT in polymer composites and adding more than this weight percentage no significant change in peaks of central deflection is observed. The reason is that, the thermal expansion coefficients of nanocomposite decreases as weight percentage of carbon nanotube changes from 0 to 1% while increases when the weight of carbon nanotubes is more than 1%.

Effect of temperature rise parameter on the nonlinear dynamic response of a multi-phase laminated composite plate reinforced with SWCNT for different plate aspect ratio are depicted in Fig. 7. The temperature field is assumed to be varied uniformly through the thickness of the plate. Three aspect ratio, *a/h*=5, 10 and 20 are considered. As may be observed, the effect of temperature rise is more prominent in thick plates rather than in thin plates. Effect of the temperature distribution on the nonlinear dynamic response of a multi-phase laminated composite plate reinforced with SWCNT for different temperature changes is presented in Fig. 8. Three type of distribution of temperature through the thickness of the plate namely, uniform linear and nonlinear are considered. As may be observed, the central deflection of the plate is maximum under uniform distribution, followed by linear and nonlinear distribution. It should be noted that, as temperature changes increases difference between curves for temperature distributions increase. Three type of distribution of temperature through the thickness of the plate namely, uniform linear and nonlinear are considered. As may be observed, the central deflection of the plate is maximum under uniform distribution, followed by linear and nonlinear distribution. It should be noted that, as temperature changes increases difference between curves for temperature distributions increase.

3.2.3 Effect of foundation stiffness

Effect of the foundation stiffness on the nonlinear dynamic response of a multi-phase laminated composite plate reinforced with CNT is analyzed in this section.

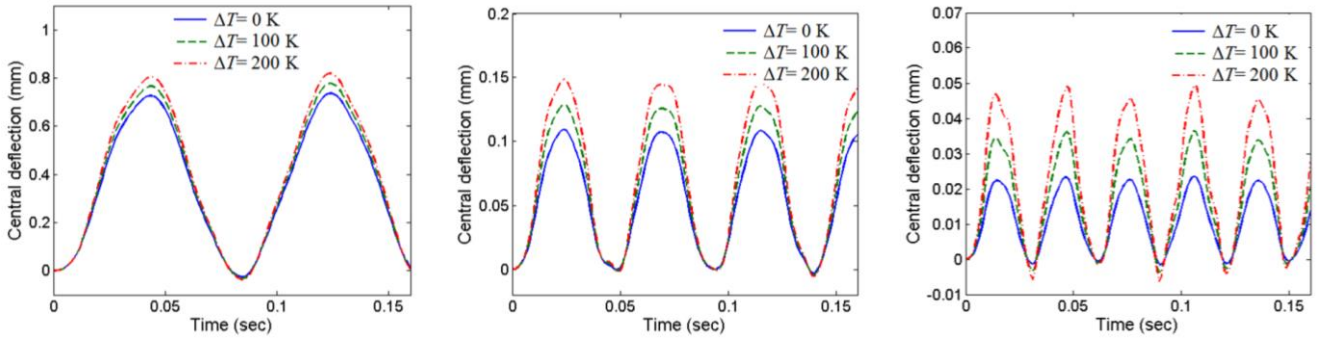

Fig. 7 Effect of temperature rise for different plate aspect ratio on the central deflection of a simply supported multi-phase laminated composite plate reinforced with SWCNT for different plate aspect ratio (a) a/h=20; (b) a/h=10; (c) a/h=5

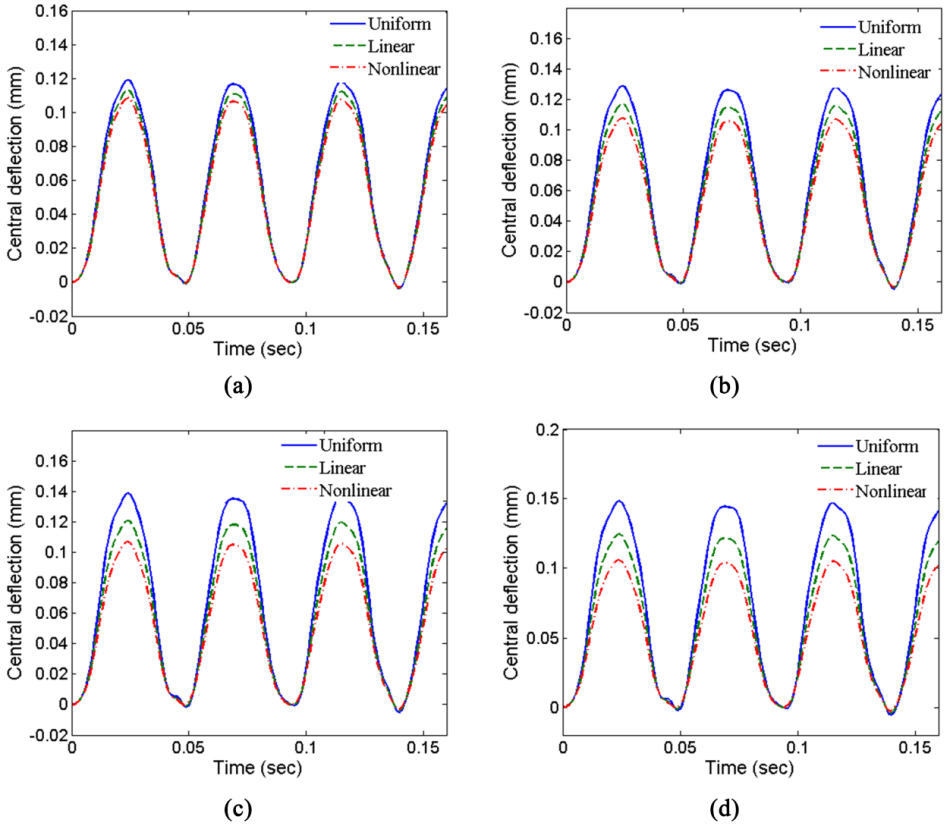

Fig. 8 Effect of temperature distribution on the central deflection of a simply supported multi-phase laminated composite plate reinforced with SWCNT for different temperature changes (a) ΔT=50 K; (b) ΔT=100 K; (c) ΔT=150 K; (d) ΔT=200 K

Plate is assumed at reference temperature. Two foundation models are considered. The stiffness are (K_w, K_s)=(1000, 0) for the Winkler elastic foundation, (K_w, K_s)=(1000, 100) for the Pasternak elastic foundation and (K_w, K_s)=(0, 0) for the plate without any elastic foundation. Numerical results of this section are provided in Fig. 9. Weight percentage of single walled carbon nanotube w_{cn}=3% is considered. Specifications are the same with the preceding section. As may be observed, the central deflection of the plate has decreased considerably due increasing the foundation stiffness.

3.2.4 Effect of shape of impulsive load

Effect of shape of impulsive loads on the nonlinear dynamic response of a multi-phase laminated composite plate reinforced with CNT for different stacking sequence are provided in Fig. 9. Four types of impulsive loads are considered, namely the step, triangular, half-sine and exponential pulses. Weight percentage of single walled carbon nanotube w_{cn}=1%, and volume fraction of fibers V^F=0.6 is considered. As may be observed, the step pulse produces the largest displacement amplitude for the plate with any type of stacking sequence, whereas the exponential pulse leads to the smallest amplitude. Also, as the external load is eliminated (t_0=7 s), the oscillations of the center point perform around the equilibrium position in a symmetric manner. In the case of the composite subjected to the half-sine impulsive load, the center point of the plate

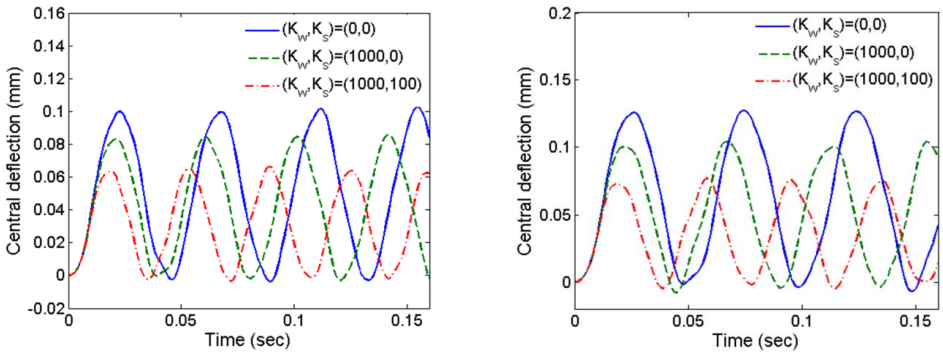

Fig. 9 Effect of the foundation stiffness on the central deflection of a simply supported multi-phase laminated composite plate reinforced with SWCNT (a) ΔT=50 K; (b) ΔT=200 K

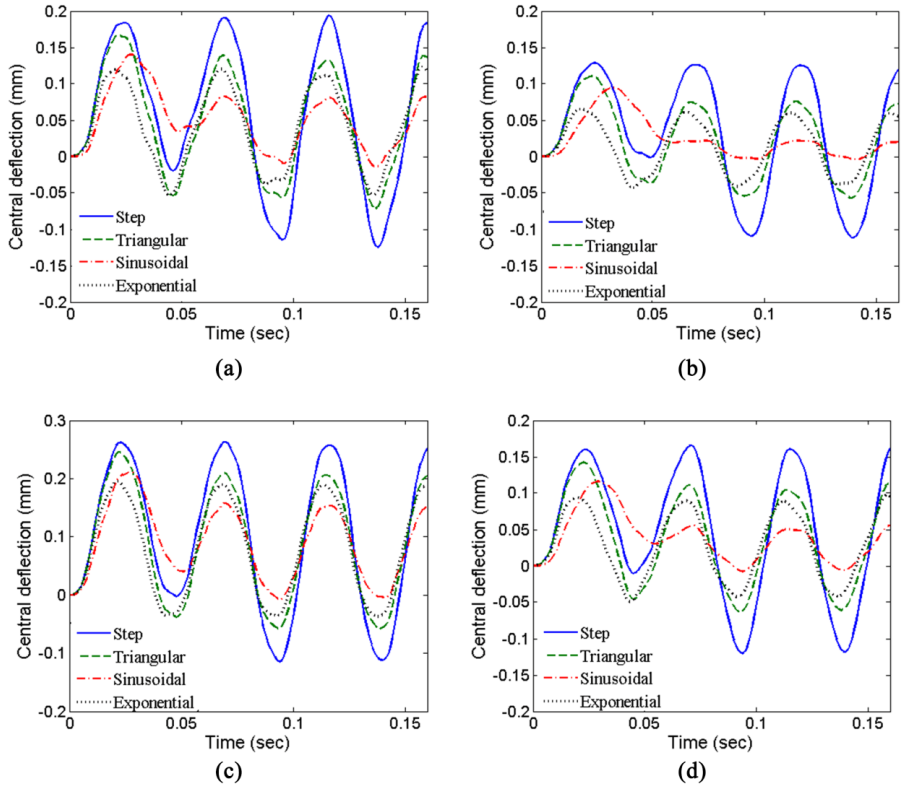

Fig. 10 Effect of shape of impulsive loads on the central deflection of a simply supported multi phase laminated composite plate reinforced with SWCNT for different stacking sequence. (a) [45°/45°/45°/45°]; (b) [0°/90°/90°/0°]; (c) [90°/0°/0°/90°]; (d) [30°/60°/60°/30°]

is always higher than the static equilibrium position. Also, the peak central deflection of the plate is maximum for [90°/0°/0°/90°] composite plate, followed by [45°/45°/45°/45°], [30°/60°/60°/30°] and [0°/90°/90°/0°] composites.

4. Conclusions

Present study is devoted to investigate the dynamic bending answers of multiscale polymer-CNT-fiber nanocomposite rectangular plates with respect to strain nonlinearities. The structure is considered to be embedded on a Winkler-Pasternak medium. Moreover, the kinematic relations are extended in the framework of an inverse cotangential plate theory to capture shear deformation effects. Homogenization procedure for three phase polymer-CNT-fiber nanocomposite material is performed according to a two-step method including Halpin-Tsai model and a micromechanics approach. Finally, the governing equations are solved based on the Newmark's method. Herein, the most important highlights of the article are going to be reviewed to put emphasize on the significance of each participant variant:

- In the situation that the plate is subjected to a dynamic loading, the maximum central deflection of the plate becomes smaller whenever the mass fraction of the CNTs is added.

• CNT aspect ratio plays a significant role influencing the dynamic behavior, but only for SWCNT reinforced composite plates. It should be noted that for composite plate reinforced with short CNT (aspect ratio less than 50) this influence is insignificant.

• The temperature distribution (uniform, linear, nonlinear) have a significant effect on the nonlinear dynamic response of a multi-phase laminated composite plate reinforced carbon nanotube. Actually, the bending responses of plates can be increased by subjecting the structure to a temperature change.

• It is clear that the maximum central deflection of the plate lessens once the nonlinear temperature change is applied. It is notable that the greatest response corresponds with the uniform temperature profile.

• Central deflection of plate is reduced using a maximum of 1% of CNT in polymer composites and adding more than this weight percentage no significant change in peaks of central deflection is observed.

• The step pulse produces the largest displacement amplitude for the plate with any type of stacking sequence, whereas the exponential pulse leads to the smallest amplitude.

• The effect of adding foundation coefficients on the central deflection of the plate is a decreasing effect. In other words, the maximum deflection decreases while both Winkler and Pasternak springs are utilized. The reason is the applied raise in the total stiffness of the system in such conditions which leads to smaller bending responses.

References

Alizada, A.N., Sofiyev, A.H. and Kuruoglu, N. (2012), "Stress analysis of a substrate coated by nanomaterials with vacancies subjected to uniform extension load", *Acta Mechanica*, **223**(7), 1371-1383.

Aydogdu, M. (2009), "A new shear deformation theory for laminated composite plates", *Compos. Struct.*, **89**(1), 94-101.

Chien, R.D. and Chen, C.S. (2006), "Nonlinear vibration of laminated plates on an elastic foundation", *Thin Wall. Struct.*, **44**(8), 852-860.

Civalek, Ö. and Demir, C. (2016), "A simple mathematical model of microtubules surrounded by an elastic matrix by nonlocal finite element method", *Appl. Math. Comput.*, **289**, 335-352.

Ebrahimi, F., Ghadiri, M., Salari, E., Hoseini, S.A.H. and Shaghaghi, G.R. (2015), "Application of the differential transformation method for nonlocal vibration analysis of functionally graded nanobeams", *J. Mech. Sci. Technol.*, **29**(3), 1207-1215.

Ebrahimi, F. and Habibi, S. (2016), "Deflection and vibration analysis of higher-order shear deformable compositionally graded porous plate", *Steel Compos. Struct.*, **20**(1), 205-225.

El Meiche, N., Tounsi, A., Ziane, N. and Mechab, I. (2011), "A new hyperbolic shear deformation theory for buckling and vibration of functionally graded sandwich plate", *Int. J. Mech. Sci.*, **53**(4), 237-247.

Ebrahimi, F. and Barati, M.R. (2016a), "Temperature distribution effects on buckling behavior of smart heterogeneous nanosize plates based on nonlocal four-variable refined plate theory", *Int. J. Smart Nano Mater.*, **7**(3), 119-143.

Ebrahimi, F. and Barati, M.R. (2016b), "Vibration analysis of smart piezoelectrically actuated nanobeams subjected to magneto-electrical field in thermal environment", *J. Vib. Control*, **24**(3), 549-564.

Ebrahimi, F. and Barati, M.R. (2016c), "Size-dependent thermal stability analysis of graded piezomagnetic nanoplates on elastic medium subjected to various thermal environments", *Appl. Phys. A*, **122**(10), 910.

Ebrahimi, F. and Barati, M.R. (2016d), "Static stability analysis of smart magneto-electro-elastic heterogeneous nanoplates embedded in an elastic medium based on a four-variable refined plate theory", *Smart Mater. Struct.*, **25**(10), 105014.

Ebrahimi, F. and Barati, M.R. (2016e), "Buckling analysis of piezoelectrically actuated smart nanoscale plates subjected to magnetic field", *J. Intel. Mater. Syst. Struct.*, **28**(11), 1472-1490.

Ebrahimi, F., Barati, M.R. and Dabbagh, A. (2016), "A nonlocal strain gradient theory for wave propagation analysis in temperature-dependent inhomogeneous nanoplates", *Int. J. Eng. Sci.*, **107**, 169-182.

Ebrahimi, F. and Dabbagh, A. (2016), "On flexural wave propagation responses of smart FG magneto-electro-elastic nanoplates via nonlocal strain gradient theory", *Compos. Struct.*, **162**, 281-293.

Ebrahimi, F. and Hosseini, S.H.S. (2016a), "Thermal effects on nonlinear vibration behavior of viscoelastic nanosize plates", *J. Therm. Stress.*, **39**(5), 606-625.

Ebrahimi, F. and Hosseini, S.H.S. (2016b), "Double nanoplate-based NEMS under hydrostatic and electrostatic actuations", *Euro. Phys. J. Plus*, **131**(5), 1-19.

Ebrahimi, F. and Barati, M.R. (2016f), "A nonlocal higher-order shear deformation beam theory for vibration analysis of size-dependent functionally graded nanobeams", *Arab. J. Sci. Eng.*, **41**(5), 1679-1690.

Ebrahimi, F. and Barati, M.R. (2016g), "Vibration analysis of nonlocal beams made of functionally graded material in thermal environment", *Euro. Phys. J. Plus*, **131**(8), 279.

Ebrahimi, F. and Barati, M.R. (2016h), "Dynamic modeling of a thermo–piezo-electrically actuated nanosize beam subjected to a magnetic field", *Appl. Phys. A*, **122**(4), 1-18.

Ebrahimi, F. and Barati, M.R. (2016i). A unified formulation for dynamic analysis of nonlocal heterogeneous nanobeams in hygro-thermal environment", *Appl. Phys. A*, **122**(9), 792.

Ebrahimi, F. and Barati, M.R. (2016j), "A nonlocal higher-order refined magneto-electro-viscoelastic beam model for dynamic analysis of smart nanostructures", *Int. J. Eng. Sci.*, **107**, 183-196.

Ebrahimi, F. and Barati, M.R. (2016k), "Hygrothermal effects on vibration characteristics of viscoelastic FG nanobeams based on nonlocal strain gradient theory", *Compos. Struct.*, **159**, 433-444.

Ebrahimi, F. and Barati, M.R. (2016l), "Buckling analysis of nonlocal third-order shear deformable functionally graded piezoelectric nanobeams embedded in elastic medium", *J. Brazil. Soc. Mech. Sci. Eng.*, **39**(3), 1-16.

Ebrahimi, F. and Barati, M.R. (2016m), "Magnetic field effects on buckling behavior of smart size-dependent graded nanoscale beams", *Euro. Phys. J. Plus*, **131**(7), 1-14.

Ebrahimi, F. and Barati, M.R. (2016n), "Buckling analysis of smart size-dependent higher order magneto-electro-thermo-elastic functionally graded nanosize beams", *J. Mech.*, **33**(1), 23-33.

Ebrahimi, F. and Barati, M.R. (2017), "A nonlocal strain gradient refined beam model for buckling analysis of size-dependent shear-deformable curved FG nanobeams", *Compos. Struct.*, **159**, 174-182.

Godara, A., Mezzo, L., Luizi, F., Warrier, A., Lomov, S.V., Van Vuure, A.W., ... and Verpoest, I. (2009), "Influence of carbon nanotube reinforcement on the processing and the mechanical

behaviour of carbon fiber/epoxy composites", *Carbon*, **47**(12), 2914-2923.

Green, K.J., Dean, D.R., Vaidya, U.K. and Nyairo, E. (2009), "Multiscale fiber reinforced composites based on a carbon nanofiber/epoxy nanophased polymer matrix: synthesis, mechanical, and thermomechanical behavior", *Compos. Part A: Appl. Sci. Manuf.*, **40**(9), 1470-1475.

Grover, N., Singh, B.N. and Maiti, D.K. (2013), "New nonpolynomial shear-deformation theories for structural behavior of laminated-composite and sandwich plates", *AIAA J.*, **51**(8), 1861-1871.

He, X.Q., Rafiee, M., Mareishi, S. and Liew, K.M. (2015), "Large amplitude vibration of fractionally damped viscoelastic CNTs/fiber/polymer multiscale composite beams", *Compos. Struct.*, **131**, 1111-1123.

Heshmati, M. and Yas, M.H. (2013), "Dynamic analysis of functionally graded multi-walled carbon nanotube-polystyrene nanocomposite beams subjected to multi-moving loads", *Mater. Des.*, **49**, 894-904.

Hu, N., Qiu, J., Li, Y., Chang, C., Atobe, S., Fukunaga, H., ... and Yuan, W. (2013), "Multi-scale numerical simulations of thermal expansion properties of CNT-reinforced nanocomposites", *Nanos. Res. Lett.*, **8**(1), 15.

Kant, T. and Pandya, B.N. (1988), "A simple finite element formulation of a higher-order theory for unsymmetrically laminated composite plates", *Compos. Struct.*, **9**(3), 215-246.

Kant, T., Varaiya, J.H. and Arora, C.P. (1990), "Finite element transient analysis of composite and sandwich plates based on a refined theory and implicit time integration schemes", *Comput. Struct.*, **36**(3), 401-420.

Kocaturk, T. and Akbas, S.D. (2013), "Wave propagation in a microbeam based on the modified couple stress theory", *Struct. Eng. Mech.*, **46**(3), 417-431.

Kim, M., Park, Y.B., Okoli, O.I. and Zhang, C. (2009), "Processing, characterization, and modeling of carbon nanotube-reinforced multiscale composites", *Compos. Sci. Technol.*, **69**(3-4), 335-342.

Lei, Z.X., Zhang, L.W. and Liew, K.M. (2015), "Elastodynamic analysis of carbon nanotube-reinforced functionally graded plates", *Int. J. Mech. Sci.*, **99**, 208-217.

Lei, Z.X., Zhang, L.W., Liew, K.M. and Yu, J.L. (2014), "Dynamic stability analysis of carbon nanotube-reinforced functionally graded cylindrical panels using the element-free kp-Ritz method", *Compos. Struct.*, **113**, 328-338.

Levinson, M. (1980), "An accurate, simple theory of the statics and dynamics of elastic plates", *Mech. Res. Commun.*, **7**(6), 343-350.

Lo, K.H., Christensen, R.M. and Wu, E.M. (1977), "A high-order theory of plate deformation-Part 1: Homogeneous plates", *J. Appl. Mech.*, **44**(4), 663-668.

Mantari, J.L., Oktem, A.S. and Soares, C.G. (2011), "Static and dynamic analysis of laminated composite and sandwich plates and shells by using a new higher-order shear deformation theory", *Compos. Struct.*, **94**(1), 37-49.

Mantari, J.L., Oktem, A.S. and Soares, C.G. (2012), "A new higher order shear deformation theory for sandwich and composite laminated plates", *Compos. Part B: Eng.*, **43**(3), 1489-1499.

Mindlin, R.D. (1951), "Influence of rotatory inertia and shear on flexural motions of isotropic, elastic plates", *J. Appl. Mech.*, **18**, 31.

Moradi-Dastjerdi, R., Foroutan, M. and Pourasghar, A. (2013), "Dynamic analysis of functionally graded nanocomposite cylinders reinforced by carbon nanotube by a mesh-free method", *Mater. Des.*, **44**, 256-266.

Murthy, M.V.V. (1981), "An improved transverse shear deformation theory for laminated antisotropic plates", Technical Report, NASA, United States.

Rafiee, M., He, X.Q., Mareishi, S. and Liew, K.M. (2014), "Modeling and stress analysis of smart CNTs/fiber/polymer multiscale composite plates", *Int. J. Appl. Mech.*, **6**(03), 1450025.

Rafiee, M., Liu, X.F., He, X.Q. and Kitipornchai, S. (2014), "Geometrically nonlinear free vibration of shear deformable piezoelectric carbon nanotube/fiber/polymer multiscale laminated composite plates", *J. Sound Vib.*, **333**(14), 3236-3251.

Rafiee, M., Yang, J. and Kitipornchai, S. (2013), "Large amplitude vibration of carbon nanotube reinforced functionally graded composite beams with piezoelectric layers", *Compos. Struct.*, **96**, 716-725.

Reddy, J.N. (1984), "A simple higher-order theory for laminated composite plates", *J. Appl. Mech.*, **51**(4), 745-752.

Reddy, J.N. (2004), *Mechanics of Laminated Composite Plates and Shells: Theory and Analysis*, CRC press.

Reissner, E. (1945), "The effect of transverse shear deformation on the bending of elastic plates", *J. Appl. Mech.*, A69-A77.

Sahoo, N.G., Rana, S., Cho, J.W., Li, L. and Chan, S.H. (2010), "Polymer nanocomposites based on functionalized carbon nanotubes", *Prog. Polym. Sci.*, **35**(7), 837-867.

Shen, H.S. (2009), "A comparison of buckling and postbuckling behavior of FGM plates with piezoelectric fiber reinforced composite actuators", *Compos. Struct.*, **91**(3), 375-384.

Shen, H.S., Yang, J. and Zhang, L. (2000), "Dynamic response of Reissner-Mindlin plates under thermomechanical loading and resting on elastic foundations", *J. Sound Vib.*, **232**(2), 309-329.

Soldatos, K.P. (1992), "A transverse shear deformation theory for homogeneous monoclinic plates", *Acta Mechanica*, **94**(3-4), 195-220.

Spitalsky, Z., Tasis, D., Papagelis, K. and Galiotis, C. (2010), "Carbon nanotube-polymer composites: chemistry, processing, mechanical and electrical properties", *Prog. Polym. Sci.*, **35**(3), 357-401.

Talha, M. and Singh, B.N. (2010), "Static response and free vibration analysis of FGM plates using higher order shear deformation theory", *Appl. Math. Model.*, **34**(12), 3991-4011.

Tornabene, F., Fantuzzi, N., Ubertini, F. and Viola, E. (2015), "Strong formulation finite element method based on differential quadrature: a survey", *Appl. Mech. Rev.*, **67**(2), 020801.

Tounsi, A., Houari, M.A. and Benyoucef, S. (2013), "A refined trigonometric shear deformation theory for thermoelastic bending of functionally graded sandwich plates". *Aerosp. Sci. Technol.*, **24**(1), 209-220.

Thostenson, E.T., Li, W.Z., Wang, D.Z., Ren, Z.F. and Chou, T. W. (2002), "Carbon nanotube/carbon fiber hybrid multiscale composites", *J. Appl. Phys.*, **91**(9), 6034-6037.

Wang, Z.X. and Shen, H.S. (2012), "Nonlinear dynamic response of nanotube-reinforced composite plates resting on elastic foundations in thermal environments", *Nonlin. Dyn.*, **70**(1), 735-754.

Yas, M.H. and Heshmati, M. (2012), "Dynamic analysis of functionally graded nanocomposite beams reinforced by randomly oriented carbon nanotube under the action of moving load", *Appl. Math. Model.*, **36**(4), 1371-1394.

Zhang, Y.C. and Wang, X. (2006), "Hygrothermal effects on interfacial stress transfer characteristics of carbon nanotubes-reinforced composites system", *J. Reinf. Plast. Compos.*, **25**(1), 71-88.

Zhu, J., Taylor, Z. and Zienkiewicz, O. (2005), "The finite element method: its basis and fundamentals", *Butterworth-Heinemann Burlington*, VT.

CC